Volume 2, Number 2, pp. 144-158, 2000.



A Structural Model of Atrial Anatomy in the Pig

A. Steingötter *, O. Dössel*, J. W. Covell***, and A. D. McCulloch**

*Institute of Biomedical Engineering, University of Karlsruhe, 76128 Karlsruhe, Germany Departments of Bioengineering** and Medicine***, University of California San Diego, La Jolla, CA 92093-0412, USA

Correspondence: steingoetter@biomed.ee.ethz.ch

Abstract. This paper describes the measurement of a data set used to create a three-dimensional (3-D) parametric model of atrial anatomy. A short introduction to porcine and human atrial anatomy is given and important anatomical differences are noted. The data acquisition techniques are described. A pig heart was arrested in diastole and perfusion fixed in-situ at physiological pressures with the chest open but the pericardium intact, then excised, cast and mounted. A six-degree-of-freedom measurement arm was used to measure three-dimensional epicardial surface geometry and fiber angles. An epicardial surface model was created using a computer aided design (CAD) software program for reverse engineering. The model was used to direct the dissection of the heart into small tissue blocks from which endocardial fiber angles and wall thicknesses were measured. Tissue blocks were then cryosectioned for histology and the identification of conducting system structures. Figures and images illustrate the resulting surface model, the acquired fiber angles and wall thickness. This preliminary work provides a foundation for building a three-dimensional anatomically detailed model suitable as a mesh for computational analysis of atrial mechanics and electrophysiology.

Keywords: Atrial anatomy, atrial modeling

Introduction

A major objective of cardiac bioengineering is to understand and simulate the electromechanical behavior of the heart. The creation of computational models of cardiac architecture and physiological function provides a means of achieving these objectives. For the quantitative analysis of many aspects of integrated cardiac function, a realistic and detailed description of cardiac anatomy is needed. Such a realistic anatomical description should describe internal and external structures of the atria and ventricles, cardiac wall thickness, myocardial fiber orientation, coronary arterial and venous networks, the morphology of the conduction system, the distribution of autonomic nerves and other histological information.

Previous work on modeling cardiac anatomy has concentrated primarily on the ventricles, especially the left ventricle, due to the critical role of these chambers in maintaining cardiac

pump function and the high mortality associated ventricular fibrillation. However, atrial arrhythmias such as atrial flutter and atrial tachycardia are prevalent and carry a risk of morbidity and mortality, especially due to thromboembolism and stroke. Because of the complex anatomy and fiber architecture of the atria, previous techniques used to model ventricular anatomy need to be substantially revised.

The purpose of this paper is to present the measurement of a data set for the creation of a parametric three-dimensional (3-D) model of atrial geometry and fiber architecture. The model is intended to will as an anatomical mesh for the simulation of atrial mechanical and electrical function. A short introduction on porcine and human atrial anatomy is given and some anatomical differences between the two species are noted. The preparation of the pig heart and the strategy to acquire the necessary data are described. Finally, the strengths and limitations of the approach are discussed and future directions are suggested.

Atrial Anatomy in Pig and Human

Due to the dissimilar postures of man and pig, the pig heart and the human heart have a different orientation in the thorax and a different shape. The posterior and anterior surfaces of the pig heart and human hearts are also located differently within the thorax. Nonetheless both have an apex and a base, with upper and lower borders of unequal size [1], [3], [4]. In the following, the anatomy of the atria of the human heart and the pig heart is described and prominent anatomical differences are pointed out.

Right Atrium

External Morphological Structures

The two caval veins, the superior vena cava (SVC) and the inferior vena cava (IVC), and the coronary sinus (CS) drain deoxygenated blood into the right atrial chamber. The porcine inferior and superior caval veins usually open into the atrium at almost right angles to one another, whereas in man the orifices are almost directly in line [1], [4].

The right atrial appendage (RAA) or right auricle is the appendicular portion of the right atrium that externally originates from the terminal groove. In the pig heart the RAA has a wide tubular appearance and extends and faces directly in the anterior direction. In man, the RAA has a characteristic triangular shape and joins the venous component over a broader area. Both in man and pig, the right atrial appendages are lined internally by pectinate muscles that originate from the terminal crest [1], [2], [3], [4].

The venous sinus or sinus venarum is the smooth-walled posterior portion of the right atrium which receives the IVC and SVC and the orifice of the coronary sinus. Viewed externally it is relatively small, extending between the terminal groove and the interatrial groove (Waterston's groove). The Waterston's groove is the infolding between the venous sinus and the right pulmonary veins of the left atrium. The major muscle bundle of the venous sinus, covering the surface of the sinus between the Waterston's groove and the terminal groove is called intercaval bundle [1], [2], [5].

Internal Morphological Structures

The tricuspid valve, between the right atrium and right ventricle, has leaflets supported by the smooth walled, muscular vestibule and the surrounding fibrous body of the heart. The largest muscular bundle in the right atrium is the terminal crest or crista terminalis. It is a longitudinal muscular ridge that originates from the anterior aspects of the septum, swings in front of the orifice of the SVC and continues downwards to the right of the orifice of the cavae [2], [3], [5]. The terminal crest gives rise to the pectinate muscles and separates the pectinate lining of the appendage from the smooth walls of the venous sinus [1], [2], [3], [5].

The natural pacemaker, the sinoatrial (SA) node or sinus node is situated subepicardially in the superior region of the terminal crest at the junction of the SVC and the right atrial appendage [6], [7], [8], [1]. In pig and human, it usually contains more collagen and connective tissue than surrounding tissue [8], [6], [9], [10].

The interatrial septum is the muscular wall separating the interior of the right and left atrium. It mainly consists of the flap valve of the oval fossa. The oval fossa or fossa ovalis is an oval depression. It represents a fetal foramen (hole) in the septum which allowed blood to pass from the right atrium to the left atrium. The principal muscles of the atria attach to the rim of the oval fossa. The inferior part of the rim is the true muscular interatrial structure, known as the sinus septum. It separates the orifice of the coronary sinus from that of the inferior caval vein and gives rise to the fibromuscular valve guarding the IVC, the Eustachian valve [1], [2], [3]. The septal region of the pig is longer than in man. This is a result of the different atrial morphology and also the apparent anterior displacement of the porcine aortic trunk compared with that of man.

Anteriorly, the sinus septum is continuous with the atrioventricular septum which contains the apex of the surface of the triangle of Koch. The entire atrial component of the atrioventricular conduction tissues is contained within the confines of the triangle [3], [7], [6], [11], [12]. The atrioventricular (AV) node is located in an interatrial position some distance above the tricuspid attachment. The AV bundle penetrates directly at the apex of the triangle of Koch [3], [11], [9], [12].

Left Atrium

External Morphological Structures

The pulmonary veins (PVs) bring oxygenated blood from the lungs to the left atrium [3], [4], [1]. The porcine left atrium receives only two pulmonary veins, where as the human left atrium receives four PVs. A prominent left azygous vein (LAZV) enters on the left side of the pig heart. Below and to the left of the upper left pulmonary vein, the LAZV drains into the coronary sinus. The comparable vessel in normal human heart is much reduced. It only persists as the left atrial oblique vein (or left superial caval vein) so that it normally drains only venous return from a small part of the left atrial musculature [1].

The left atrial appendage (LAA) or left auricle is the appendicular portion of the left atrium. In the pig it has a triangular shape and is of similar size to the right atrial appendage, whereas in human it is of tubular shape and smaller than the right atrial appendage. As in the RAA, the LAA is lined internally by pectinate muscles. In pig and man, the pectinate muscles of the LAA are restricted to the internal walls [1], [2], [3].

The principal muscular bundles of the left atrial wall are the left extremity of the interatrial bundle, or Bachmann's bundle, and the septopulmonary bundle. The septoplumonary bundle belongs to the sinus in the left atrium [2], [5].

Internal Morphological Structures

The atrioventricular valve between the left atrium and the left ventricle is called the mitral or bicuspid valve. As in the right atrium, the valve is supported by the smooth-walled, muscular vestibule and by the surrounding fibrous ring [1], [2], [3].

Coronary Circulation

The circumferential groove that separates the atrial musculature from the ventricular musculature is called the atrioventricular (AV) groove or coronary sulcus. Right and left circumferential coronary artery lie in this groove. It is incomplete anteriorly and most marked on the right lateral side.

The coronary arterial circulation of the pig is similar to man, whereas the anatomy of the coronary venous return is very different from that of the human heart [1]. The most noticeable example is that no right azygous vein can be found in the porcine heart. Instead a prominent left azygous vein (LAZV) drains venous blood into the coronary sinus.

Methods

Animal and Tissue Preparation

All procedures were conducted according to the NIH Institute for Laboratory Animal Research, 'Guide to the Care and Use of Laboratory Animals'. Procedures were reviewed and approved by the UCSD Animal Subjects Committee.

The pig heart was perfusion fixed *in-situ* for 10 minutes using 10% glutaraldehyde. It was isolated with the pericardium intact and parts of the trachea and the lungs attached. Immediately after the excision, it was placed in a bath with 10% formalin and was perfusion fixed *in-vitro* for another 30 minutes using 10% formalin. Physiological atrial pressures of 5 mmHg for the right atria and 10 mm Hg for the left atria were applied during perfusion fixation [13], [14]. The heart was then immersed in 10% buffered formalin and stored there for one day. Then, the fixed heart was cleaned from tracheal and lung tissue.

The pericardium was removed and the blood vessels were trimmed. Silicone elastomer that slowly polymerizes over a period of approximately 48 hours was used to fill the chambers of the pig heart and thus to create a cast. The viscosity of the silicone elastomer did not allow to injected the material through atrial vessels without risk of causing major damage to the atrial walls. Therefore, holes were cut into the right and left ventricle from where the silicone elastomer was injected via tubing into the right and left atria, respectively. After atria and ventricles were filled, two parallel square metal posts were stuck into the silicone cast through the two holes in the ventricles. The cast heart was again immersed in 10% buffered formalin with its apex pointing upwards. The heart became securely mounted on the posts after the silicone had set, see Figure 1.



Figure 1. Anterior view of the mounted and cast pig heart.

Measurements

- **1.** A user-specified Cartesian `world coordinate system' for the 3-D model was established. It was defined with the 6 degree-of-freedom measurement arm that was also used to digitize the specimen. Every point in space could be digitized in reference to the fixed measurement arm and the defined world coordinate system. In addition, a local coordinate system was created on the stand of the heart to facilitate the display and monitoring of the actual digitizing process.
- **2.** The 3-D surface model was created by digitizing the epicardial surface with the measurement arm. Therefore, different surface areas were defined on the heart by marking boundary lines on the epicardium, see Figure 2. Node points were recorded along these boundaries. Through an interface, the measured coordinates were transferred to a CAD

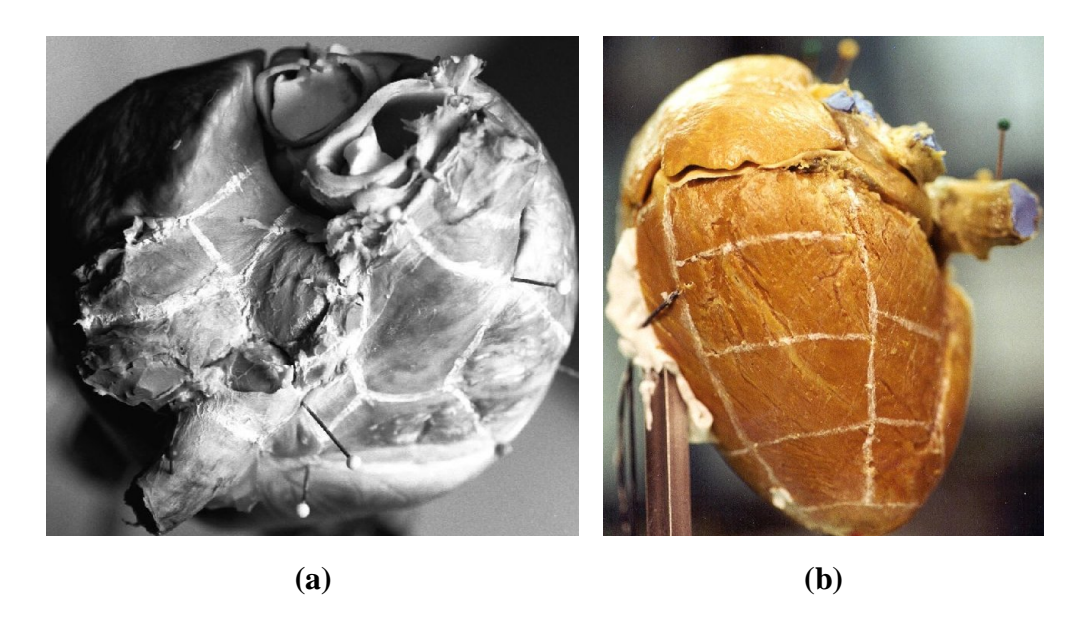


Figure 2. Fixed pig heart with marked boundary lines. (a) Boundary lines on the atria. (b) Boundary lines on the left ventricle.

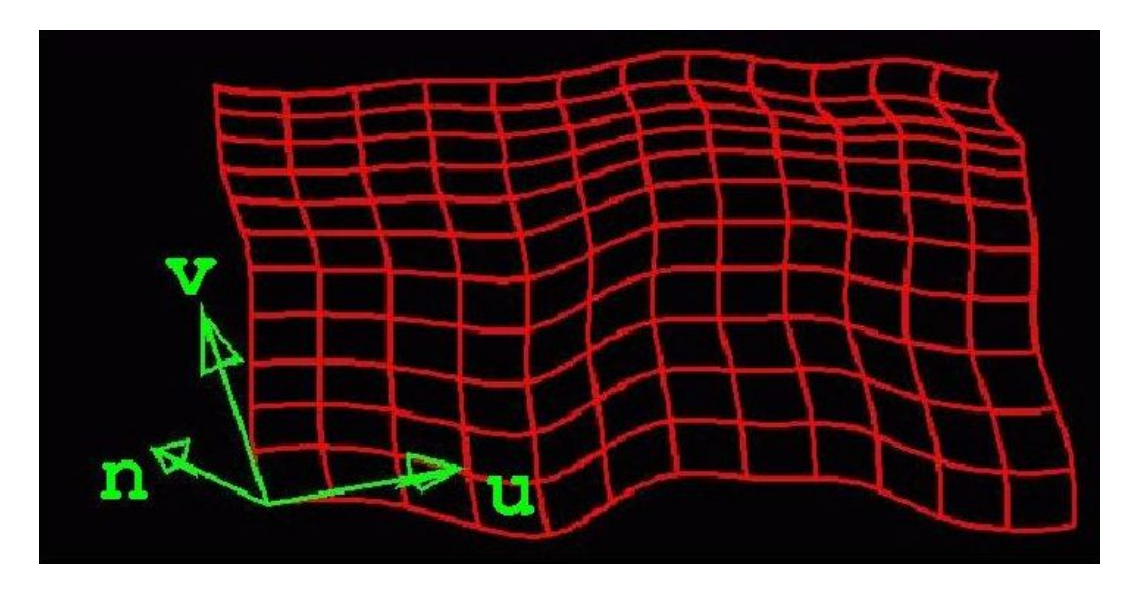


Figure 3. Parametric surface (red) represented by arrays of bicubic patches. The u and v tangent vectors and the normal vector n of the bottom left node point are displayed (green vectors).

software application. In the CAD software, splines were calculated from the digitized node points and then two-dimensional (2-D) surfaces in 3-D space were created from these splines. The surfaces were modeled as parametric bicubic spline surfaces which are represented by two surface parameters u and v, see Figure 3.

3. Fiber angles of the epicardial myocardium were measured with the 3-D measurement arm. For a better analysis of the fiber orientation, the epicardium and underlying fat and connective tissue were removed first. Fiber angles of surface node points were digitized by defining a reference position for the arm and by holding the longitudinal axis of the probe along the surface normals of these node points. Thus, the measured rotation angle (Euler angle) C around the long-axis of the probe represented the desired 2-D fiber angle **3.** See Figure 4a. Obviously, it was not possible to hold the probes long-axis exactly along the normal vectors. By calculating the original positions and directions of the probe and determining the directions of the normal vector, the fiber angles were mathematically adjusted, see Figure 4b.

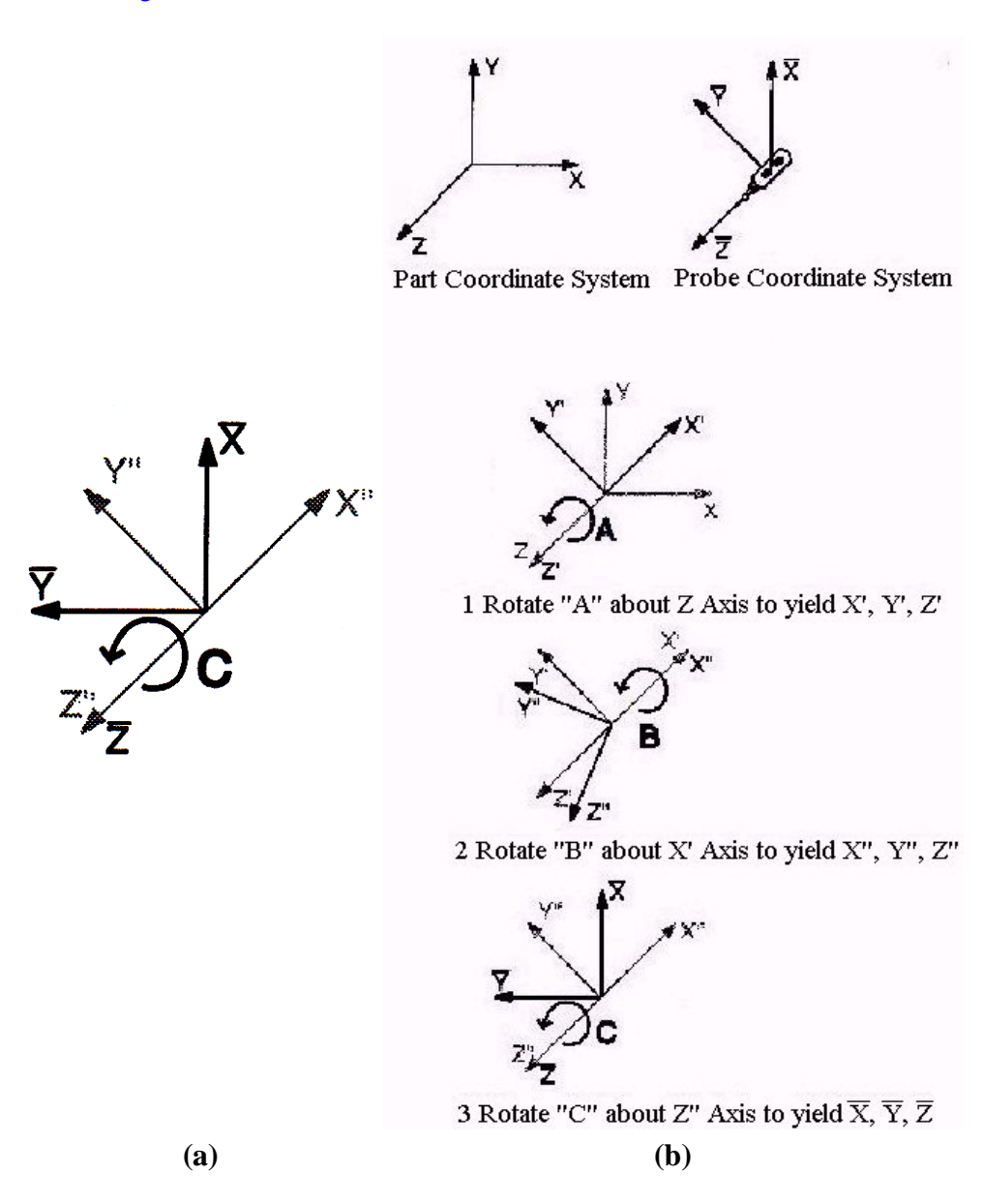


Figure 4. The rotation angles (Euler angles) of the measurement arm. (a) Rotation angle C represents the second rotation around the z-axis of the probe and equals the fiber angle &. (b) World Coordinate System, Probe Coordinate System and rotation angles. Rotation angle A, represents the first rotation around the z-axis (long-axis) of the probe. Rotation angle B represents the rotation around the x-axis of the probe.

4. The heart was dissected along the marked boundary lines. The dissected tissue sheets were pinned down on a cork plate with the endocardial surface facing up. The *u*, *v* directions and the normal vector of the corresponding surface and the reference line for the succeeding endocardial fiber angle measurement were marked on the cork, see Figure 5a. Epicardial boundaries, thickness data and endocardial boundaries of the flat tissue sheet were digitized, see Figure 5b. Step by step the cardiac wall was cut down into single tissue sheets. Thus, inner cardiac structures became accessible. These were digitized, then surfaces were created and were added to the 3-D surface model and fiber angles were measured. Then, the structures were dissected and wall thickness was acquired in the same way as described above. High resolution pictures were taken from every tissue sheet.

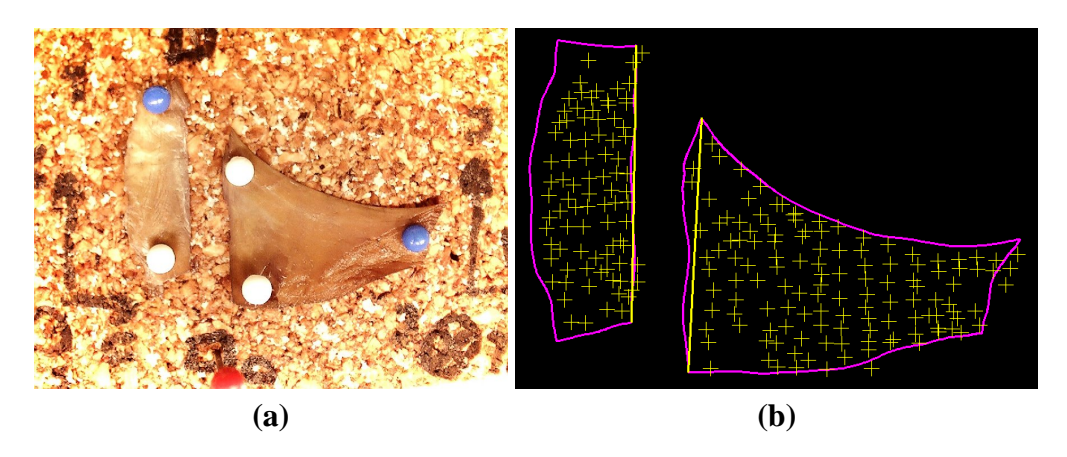


Figure 5. (a) Dissected and pinned down tissue sheets (Eustachian valve) on cork plate. (b) Digitized epicardial boundaries (purple) and thickness data points (yellow). The yellow lines indicated the reference boundaries.

- **5.** Endocardial fiber angles of intra-atrial surfaces that became accessible during the dissection were measured in the same way as described for the epicardial fiber angles, see Figure 4. In this case, the endocardium was removed for a better analysis of the fiber orientation. The endocardial fiber angles of the dissected tissue sheets were later analyzed with the microscope after histological preparation. To allow the transformation of these measured, 2-D fiber angles into 3-D space, a reference boundary was defined for each tissue sheet before dissection, see Figure 5. This boundary line had to be straight and the cut along this line had to be in the direction of the corresponding surface normals. Hence, the resulting values of the 2-D fiber angles do not change in reference to the reference boundary when imported into the 3-D surface model. The properties of this boundary in the surface model are known.
- **6.** Dissection was simulated for the 3-D surface model in the computer. The surface creation program was used to unwrap 3-D surfaces into flat panels developed from the 3-D surfaces, see Figure 6. Every surface area in the model corresponded to an epicardial surface of a tissue sheet. Hence, every developed unwrap panel represented the flat epicardial surface of a dissected tissue sheet.

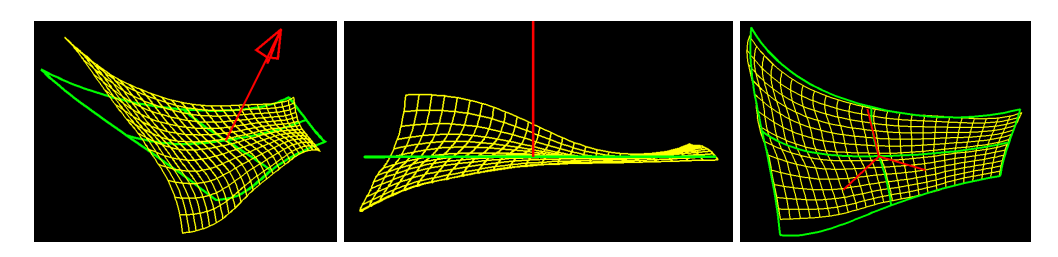


Figure 6. Different views of a surface grid (yellow) and the corresponding unwrap panel (green) with normal vector (red).

7. The measured data from the pinned down tissue sheets was registered back to the 3-D surface model. First, the acquired 2-D data sets of the sheets were imported into the data set of the model. Then, these were placed in position by matching their normal vectors and epicardial boundaries with those of the corresponding unwrap panels. Thus, a consistent data set that includes all acquired data was created, see Figure 7.

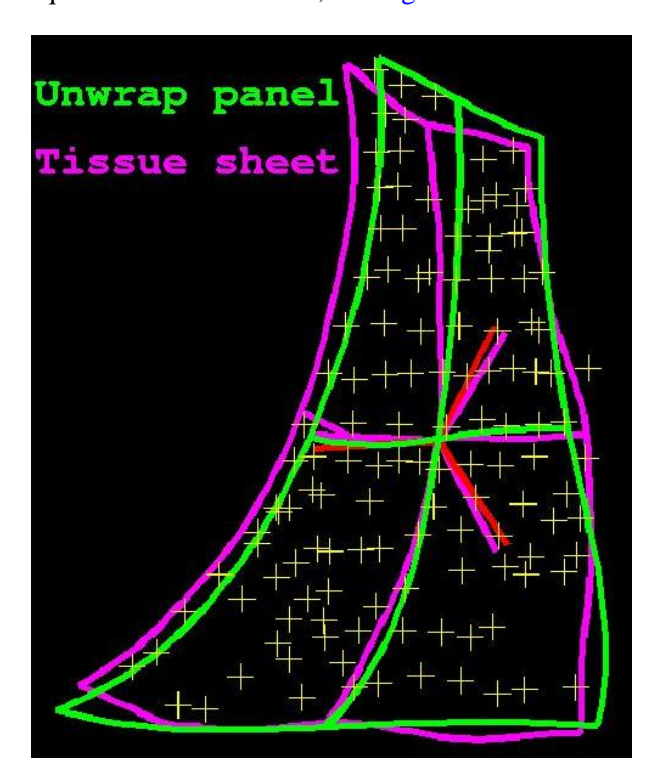


Figure 7. Tissue sheet boundaries (purple) and normal vector (red) and thickness data (green points) matched with the corresponding unwrap panel (yellow).

8. Specific tissue sheets containing nodal tissue were analyzed to determine the location of the sinoatrial (SA) node and the atrioventricular (AV) node. The terminal crest was split up where the location of the SA node was assumed. The adjacent tissue pieces to the cross sections were prepared for histological analysis [16], [17], [18], [19], [15]. The tissue pieces were sectioned in slices 15 microns thick, stained with the Masson's trichrome method and then analyzed with the microscope. The same procedure was later applied to tissue containing the AV node.

Results

A total of 70 digitizing sessions were performed to acquire data. Eleven sessions were needed to create the 3-D epicardial surface model of the pig heart. One session was used to digitize additional atrial dissection lines to represent the appendages with smaller 3-D surfaces. 13 sessions were used to digitize the epicardial fiber angles. 15 sessions were needed to add boundary or dissection lines of structures that became accessible after dissection. 23 sessions were needed to digitize the epicardial boundaries, endocardial structures and the wall thickness data of the dissected tissue sheets.

Epicardial Surface Model

A total of 112 3-D surfaces were created. 95 of these were used to create the complete anatomical model of the pig heart. 67 from the 95 surfaces represented the complete 3-D epicardial surface model of the specimen, see Figure 9. The atrial epicardial surface and accessory vessels were represented by 47 of these surfaces, see Figure 10. 24 represented the epicardium of the right atrium, 19 represented the epicardium of the left atrium and 4

represented the left azygous vein and the coronary sinus. The ventricles could be represented by only 2 surfaces (ventricles and apex) or divided in several smaller surface areas. The complete right ventricle was divided in 8 surface areas, see Figure 11b. The posterior part of the left ventricle was also divided in 8 surfaces, see Figure 11a. Inner right and left atrial and septal surfaces were represented by 27 surfaces. One surface represented the inner wall of the coronary sinus.

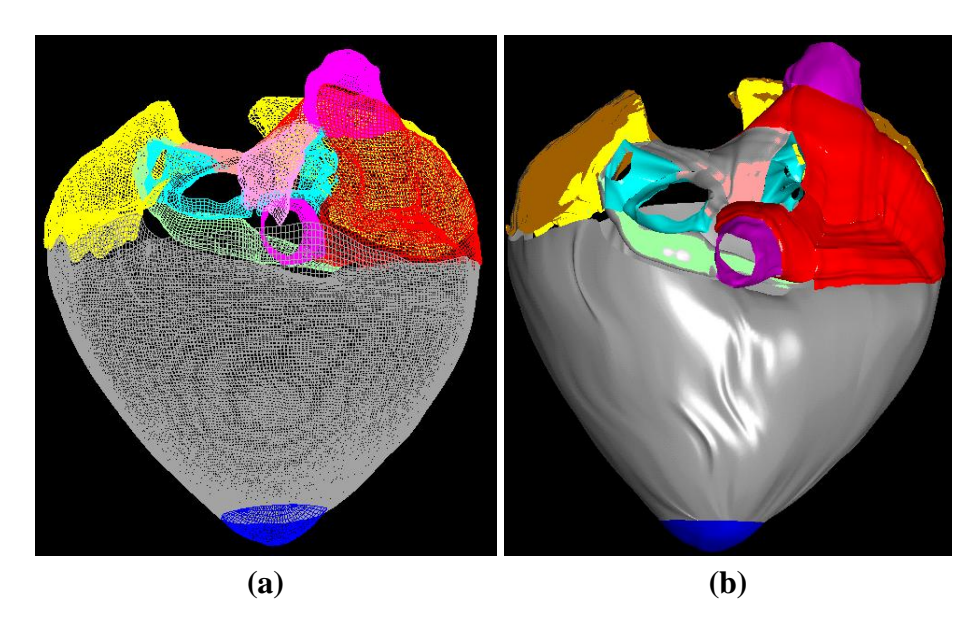


Figure 9. Final 3-D epicardial surface model. (a) The created surfaces are represented by their u and v flowlines what results in a surface grid. (b) The created surfaces were rendered. The surfaces are displayed in different colors for a better differentiation. The colors were randomly picked. Right atrium (red), left atrium (light red), right and left atrial appendage (yellow), vena cavae (purple), pulmonary veins (light blue), coronary sinus and left azygous vein (light green), ventricles (grey), apex (blue).

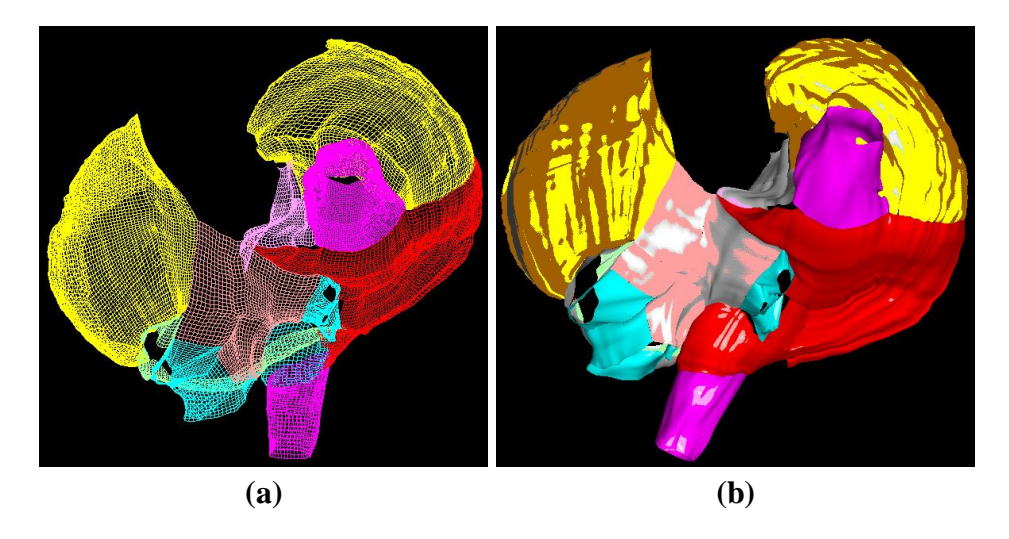


Figure 10. Created atrial epicardial surface model. (a) Surface grids. (b) Rendered surfaces. Right atrium (red), left atrium (light red), right and left atrial appendage (yellow), vena cavae (purple), pulmonary veins (light blue), coronary sinus and left azygous vein (light green).

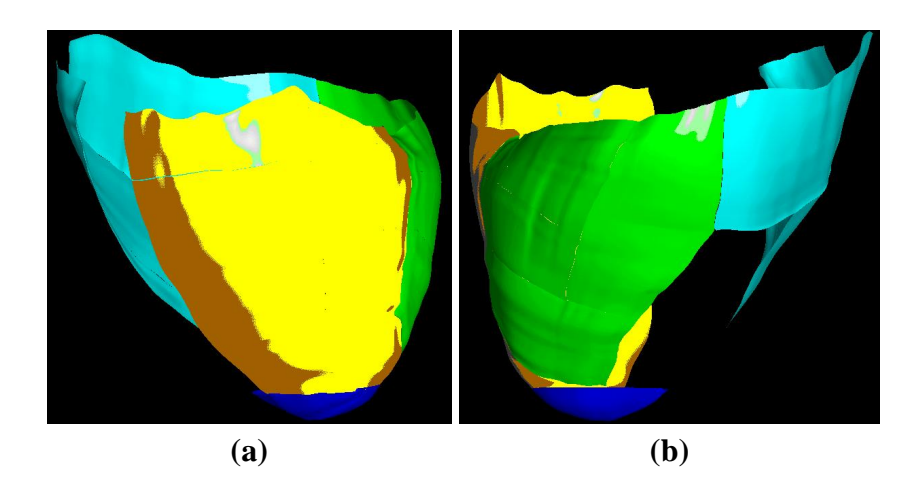


Figure 11. Subdivided right and left ventricular surface. (a) Left ventricular surfaces (blue). The posterior and lateral part of the left ventricle was subdivided into 8 smaller surfaces. (b) Right ventricular surfaces (green and white). The posterior and lateral part of the right ventricle (green) was subdivided into 8 smaller surfaces. The anterior part (white) was subdivided into 3 smaller surfaces.

Fiber Angles

Fiber angles were imported into the surface model and then projected onto the corresponding surface along the surface normals. In the following, the atrial and ventricular surface areas are displayed together with the corresponding original fiber angle points. A total of 6711 fiber angles were digitized during this project. In the following, the distribution of the digitized fiber angles is listed. 525 fiber angles for left atrial appendage (LAA), 1023 fiber angles for right atrial appendage(RAA), 922 fiber angles for right atrium (RA), SVC and IVC, 647 fiber angles for left atrium (LA) and left pulmonary vein (lPV), 439 fiber angles for right atrial wall under right PV, 106 fiber angles for Eustachian valve (EV) (see Figure 12), 448 fiber angles for region of and around triangle of Koch, 303 fiber angles for vestibular ring of RA, 650 fiber angles for vestibular ring of LA, 245 fiber angles for inner left atrial walls attached to left azygous vein (LAZV) and coronary sinus (CS), 235 fiber angles for anterior right ventricle (RV), 254 fiber angles for anterior and lateral RV, 299 fiber angles for posterior RV, 576 fiber angles for posterior left ventricle (LV).

Thickness Data

Thickness data and endocardial structures were digitized for every dissected tissue sheet that had a corresponding 3-D surface in the model. As described in section, the points were collected all over the endocardial surface in no special order. Endocardial pathways and structures were digitized as 3-D polylines. A total of 7461 thickness data points of the atrial cardiac wall were digitized during this project. In the following, the distribution of the thickness data points over the atrial surface is listed. 1092 thickness data point for left atrial appendage, 928 thickness data points for right atrial appendage, 3478 thickness data points for complete right atrium, 1052 thickness data points for right atrial wall, 470 thickness data points for SVC, 298 thickness data points for IVC, 116 and 87 thickness data points for Eustachian valve, see Figure 13, 185 thickness data points for right atrial wall under right PV, 267 thickness data points for region of and around triangle of Koch, 172 thickness data points for vestibular ring of RA, 1613 thickness data points for complete left atrium, 321 thickness data points for left atrial wall, 369 and 119 thickness data points for left PV and LAZV, 246 thickness data points for wall of right PV attached to the RA, 411 thickness data points for vestibular ring of LA, 97 and 89 thickness data points for interatrial septum and left atrial wall covering the coronary sinus, 253 thickness data points for complete coronary sinus, 153 thickness data points for posterior and free vascular wall of coronary sinus, 100 thickness data points for vascular wall of coronary sinus attached to LA wall.

Nodal Tissue

Nodal tissue of the sinoatrial (SA) node or sinus node could be determined in the terminal crest, see Figure 14. More difficult was the detection the atrioventricular nodal tissue in the atrial tissue of the triangle of Koch. Nevertheless, tissue was detected that had similar properties to nodal tissue, see Figure 15.

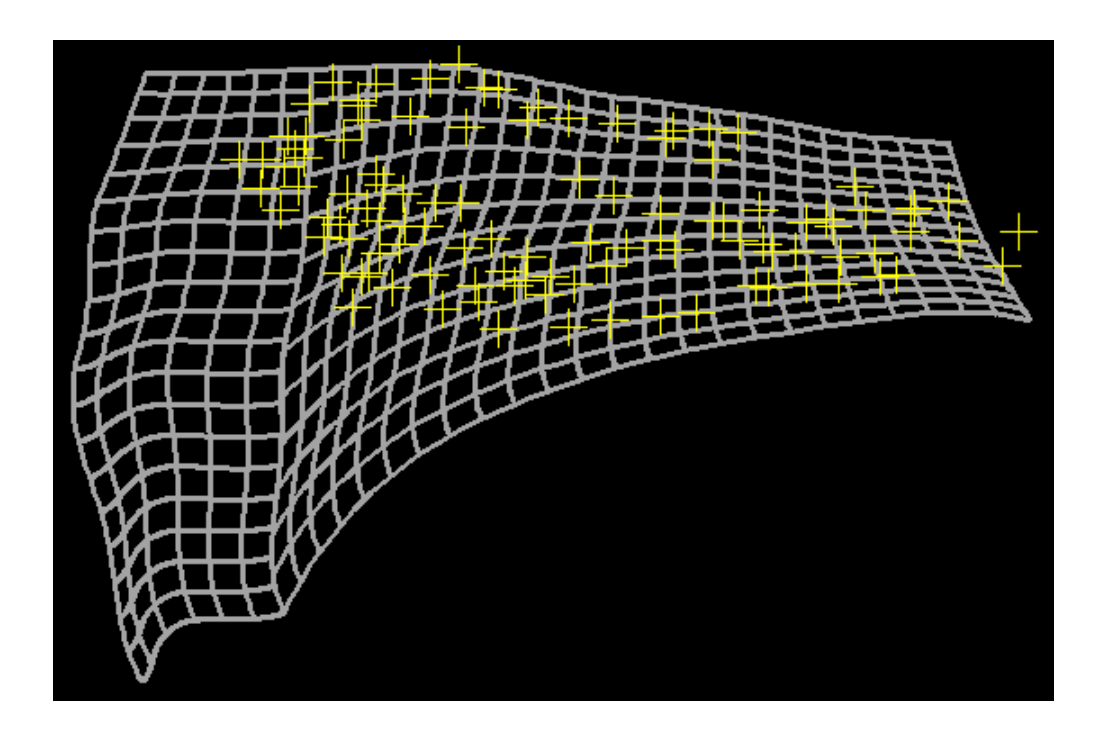


Figure 12. Digitized epicardial fiber angle node points (yellow) of the Eustachian valve (EV) with the corresponding surfaces (gray).

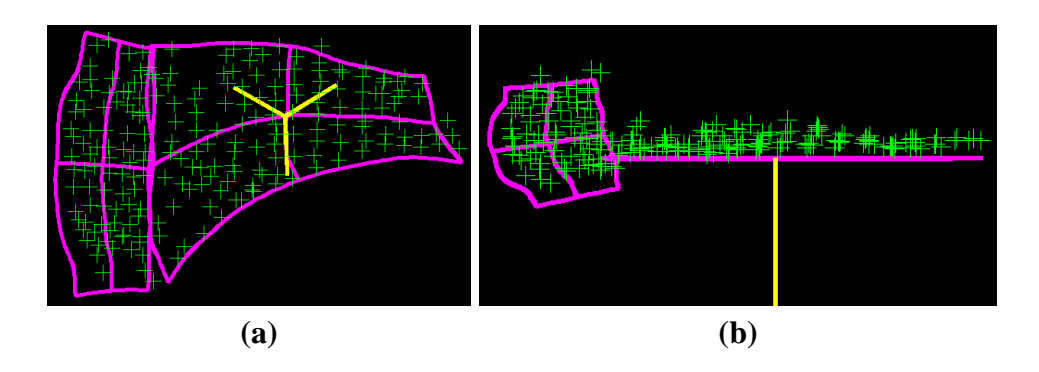


Figure 13. Digitized thickness data of the Eustachian valve and also of an adjacent part of the IVC. (a) Overview of the distribution of the digitized node points over the corresponding flat surfaces. (b) Overview of the distances of the node points from the corresponding flat surfaces.

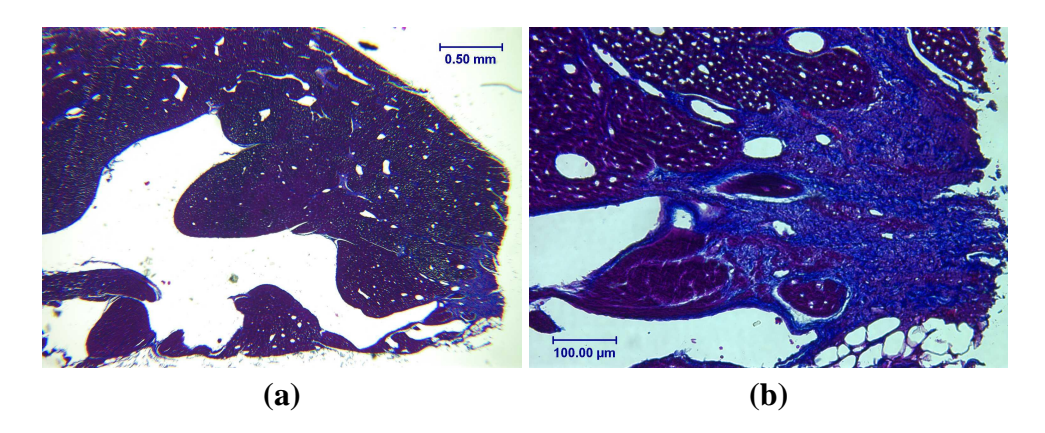


Figure 14. Stained tissue slice representing a cross section of the terminal crest. The Masson's trichrome staining method was used. Collagen is blue, muscle fibers are violet, nuclei are black. a) 4x Magnification. b) 20x Magnification.

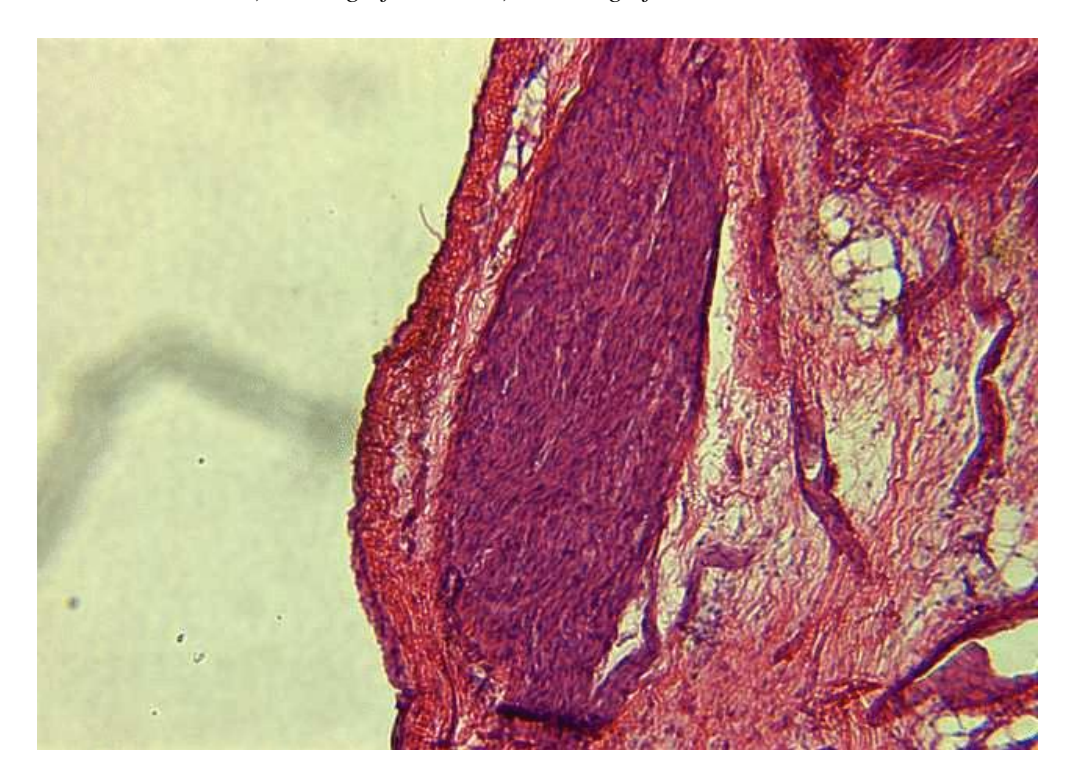


Figure 15. Stained tissue slice representing a section of the triangle of Koch. The hematoxylin and eosin staining method was used. Muscles are red, collagen is violet. 10x Magnification.

Conclusions

Advantages

Because the heart was perfusion fixed *in-situ*, non-physiological deformations of the heart could be reduced, see section Animal and Tissue Preparation. The pericardium was left intact during the perfusion fixation and also during excision. This gave additional stability to preserve the heart's shape, so that neither atrial chamber would collapse or deform.

The advantage of this project over the creation of a 3-D surface model from section images from an MRI or CT scan of an explanted heart, was that the specimen could be analyzed from any given view. Hence, complex and small cardiac structures could be analyzed more specifically and at higher spatial resolution. Cardiac muscle fibers could be visually analyzed

after cleaning the specimen from fat and connective tissue. The tissue could be histologically analyzed to get detailed information about inner myocardial structures and tissue, about muscle fiber orientations and even cardiac innervation. Using the 3-D epicardial surface model as a reference, the histological data set could be registered back to the heart.

The average precision of the created surface model is substantially better then one millimeter. This value is superior to achievable resolutions of clinical CT scans and clinical MRI images [20].

Disadvantages and Limitations

The digitizing procedure and the creation of the 3-D surface model was accomplished in about a week. The digitizing time of one or two days is long in comparison to a single MRT or CT scan.

Using the method described in this thesis, the epicardial surface model must be created first before any endocardial information can be acquired. Therefore tissue must be dissected to get access to inner atrial features. Every dissection causes indeterminate deformations in the remaining mounted tissue.

Not determinable errors occurred during the measurements and during editing the data set and creating the surfaces. The largest source of variation is the accuracy of the operator. A compromise must be made between the effort for the digitizing procedure and the achievable precision of the digitized data.

Perspectives

To complete the atrial anatomical data set, the histological analysis must be completed. Myocardial fiber orientations throughout the atrial wall must be measured and registered back to the dissected tissue sheets. Also, the nerve fiber distribution in the atrial tissue should be detected and imported to the 3-D surface model [6], [7], [8]. To include information on cardiac material properties, the percentage of collagen in the tissue should be determined.

After the histological data is acquired, the data set must be reassembled into 3-D shape.

The reassembled atrial data set could be used to create a finite element model. This would facilitate incorporating the data into existing mechanical, electrical or electromechanical cardiac models. Using the finite element program, *Continuity*, developed at UCSD, progress is already being made converting the model and measurements described in this thesis into a new finite element model.

The refined techniques could be applied to a human heart. When applying this project to a human heart, the perfusion fixation in-vivo would not be applicable. Instead, the human heart would be isolated from a donated dead body that is usually more than two days old. The heart would be in a rigid state and the vessels and chambers would contain blood clots and fibrin. Therefore, the heart must be dilated under hydrostatic pressure and rinsed with tap water to remove these blood clots and fibrin [21], [22].

Subsequently, the heart must be perfusion fixed for several hours with 10% or 20% formalin or glutaraldehyde. Depending on the thickness of its ventricular walls, the heart remains immersed for one or more days in 10% buffered formalin, where it can also be stored before further processing [21], [22]. Preparation, casting and mounting could applied in a similar way as for the pig heart.

Conclusion

The pig is an important experimental model of human atrial and ventricular pathologies including atrial arrhythmias which are becoming increasingly prevalent, especially among

elderly patients. Therefore, the current detailed anatomic measurements and the created model have the potential to be useful for providing an improved understanding of the anatomic basis of these disorders in humans. However, ultimately the present analysis should be repeated for human atria from healthy and diseased hearts. The experiences gained in the present project should make this undertaking more feasible, efficient, and accurate.

Acknowledgements

The authers wish to acknowledge Dr. James W. Covell for the use of his laboratory and Rish Pavelec and Troy for excellent surgical and technical support. We thank An Pham, Steffen Ritter, Anne Gebert and Ilka Lorenzen for support and help during the measurements.

References

- [1] Crick, S.J., Sheppard, M.N., Ho, S.Y., Gebstein L. and Anderson, R.H., "Anatomy of the pig heart: comparisons with normal human cardiac structure", Journal of Anatomy, vol. 193, pp. 105-119, 1998.
- [2] Wang, K., Ho, S.Y., Gibson, D.G. and Anderson, R.H., "Architecture of atrial musculature in humans", British Heart Journal, vol. 73, pp. 559-565, 1995.
- [3] Wilcox, B.R. and Anderson, R.H., "Surgical Anatomy of the Heart", Raven Press, New York, ISBN 0-88167-103-7, 1985.
- [4] Becker, A.E. and Anderson, R.H., "Pathology of Congenital Heart Disease", Butterworth, London, Boston, Sydney, ISBN 0-407-00137-9, 1981.
- [5] Papez, J. W., "Heart musculature of the atria", The American Journal of Anatomy, vol. 27, no. 3, pp. 255-285, 1959.
- [6] Bharati, S., Huang, S.K.S., Parr, G.V.S., Bauernfeind, R. and Lev, M., "The conduction system of the swine", Chest, vol. 100, pp. 207-12, 1991.
- [7] Crick, S.J., Sheppard, M.N., Ho S.Y. and Anderson, R.H., "Localisation and quantitation autonomic innervation in the porcine heart I: conduction system", Journal of Anatomy, vol. 195, pp. 341-357, 1999.
- [8] Bojsen-Moller, F. and Tranum-Jensen, J., "Whole-mount demonstration of cholinesterase-containing nerves in the right atrial wall, nodal tissue, and atrioventricular bundle of the pig heart", Journal of Anatomy, vol. 108, no. 3, pp. 375-386, 1971.
- [9] Anderson, R.H. and Ho, S.Y., "The architecture of the sinus node, the atrioventricular conduction axis, and the internodal atrial myocardium", Journal of Cardiovascular Electrophysiology, vol. 9, pp. 1233-1248, 1998.
- [10] Taylor, J. R. and Taylor, A. J., "The relationship between the sinus node and the right atrial appendage", Canadian Journal of Cardiology, vol. 13, no. 1, pp. 85-92, 1997.
- [11] Sanchez-Quintana, D., Davies, D.W., Ho, S.Y., Oslizlok P. and Anderson, R.H., "Architecture of the atrial musculature in and around the triangle of Koch", Journal of Cardiovascular Electrophysiology, vol. 8, pp. 1396-1407, 1996.
- [12] Cabrera, J.A., Sanchez-Quintana, D., Ho, S.Y., Medina A. and Anderson, R.H., "The architecture of the atrial musculature between the orifice of the inferior caval vein and the triscuspid valve: the anatomy of the isthmus", Journal of Cardiovascular Electrophysiology, vol. 9, pp. 1186-1195, 1998.
- [13] Stone, H.L. and Sawyer, D.C., "Cardiac output and related measurements in unanesthetized miniature swine", Swine in Biomedical Research, L.K. Bustad, R.O. McClellan, Richland, Washington: Batelle Memorial Institute, Pacific Nothwest Laboratory, pp. 411-418, 1966.
- [14] Engelhardt, W., "Swine cardiovascular physiology a review", Swine in Biomedical Research, L.K. Bustad, R.O. McClellan, Richland, Washington: Batelle Memorial Institute, pp. 307-329}, Pacific Nothwest Laboratory, 1966.
- [15] Smith, A., Yen Ho, S. and Anderson, R.H., "Histological study of the cardiac conducting system as a routine procedure", Medical Laboratory Siences, vol. 34, pp. 223-229, 1977.
- [16] Bancroft, J.D. and Pearse, A.G.E., "An introduction to histochemical technique", Butterworth, London, 1, 1967.
- [17] Gurr, E., "Staining, practical and theoretical", The Williams and Wilkins Co., Baltimore, 1, 1962.
- [18] Bancroft, J.D. and Stevens, A., "Theory and practice of histological techniques", Churchill Livingstone, New York, Edinburgh, London, Madrid, Melbourne, 4, ISBN 0-443-04760-X, 1996.
- [19] Bancroft, J.D. and Pearse, A.G.E., "An introduction to histochemical technique", Butterworth, London, 1, 1967.
- [20] Morneburg, H., "Bildgebende Systeme f
 ür die medizinische Diagnostik", PUBLICIS MCD, M
 ünchen, 3, ISBN 3-89578-002-2, 1995.

- [21] Tiedemann, K. and von Hagens, G., "The technique of heart plastination", Anatomical Record, vol. 204, no. 3, pp. 295-299, 1982
- [22] von Hagens, G., Tiedemann, K. and Kriz, W., "The current potential of plastination, anatomy and embryology", vol. 175, no. 4, pp. 411-421, 1986.



Official journal of the International Society for Bioelectromagnetism